Radiology: Cardiothoracic Imaging

ORIGINAL RESEARCH

T2-weighted Lung Imaging Using a 0.55-T MRI System

Adrienne E. Campbell-Washburn, PhD • Ashkan A. Malayeri, MD • Elizabeth C. Jones, MD, MPH • Joel Moss, MD, PhD • Kevin P. Fennelly, MD, MPH • Kenneth N. Olivier, MD, MPH • Marcus Y. Chen, MD

From the Cardiovascular (A.E.C.W., M.Y.C.) and Pulmonary (J.M., K.P.F., K.N.O.) Branches, Division of Intramural Research, National Heart, Lung, and Blood Institute, National Institutes of Health, Department of Health and Human Services, Building 10, Room BID-47, 10 Center Dr, Bethesda, MD 20892; and Department of Radiology and Imaging Sciences, Clinical Center, National Institutes of Health, Department of Health and Human Services, Bethesda, Md (A.A.M., E.C.J.). Received December 11, 2020; revision requested January 22, 2021; revision received April 22; accepted May 4. **Address correspondence to** A.E.C.W. (e-mail: *adrienne.campbell@nih.gov*).

Supported by the NHLBI Division of Intramural Research (Z01-HL006257).

Conflicts of interest are listed at the end of this article.

Radiology: Cardiothoracic Imaging 2021; 3(3):e200611 • https://doi.org/10.1148/ryct.2021200611 • Content codes: CH MR

Purpose: To assess a 0.55-T MRI system for imaging lung disease and to compare image quality with clinical CT scans.

Materials and Methods: In this prospective study conducted between November 2018 and December 2019, respiratory-triggered T2-weighted turbo spin-echo MRI at 0.55 T was compared with clinical CT scans in 24 participants (mean age, 59 years ± 16 [standard deviation]; 18 women) with common lung abnormalities. MR images were reviewed and scored by experienced readers. Abnormal findings identified with MRI and CT were compared using the Cohen κ statistic.

Results: High-quality structural pulmonary MR images were attained with an average acquisition time of 11 minutes ± 3. MRI generated sufficient image quality to robustly detect bronchiectasis (κ = 0.61), consolidative opacities (κ = 1.00), cavitary lesions (κ = 1.00), effusion (κ = 0.64), mucus plug (κ = 0.68), and solid scattered nodularity (κ = 0.82). Diffuse disease, including ground-glass opacities (κ = 0.57) and tree-in-bud nodules (κ = 0.48), were the findings that were most difficult to discern using MRI, with false readings in four of 18 patients for each feature. Nodule size, which was measured independently at CT and MRI, was strongly correlated (R^2 = 0.99) for nodules with a measurement of 10 mm ± 5 (range, 5–23 mm).

Conclusion: This initial study indicates that high-performance 0.55-T MRI holds promise in the evaluation of common lung disease.

Clinical trials registration no. NCT03331380

Supplemental material is available for this article.

Clinical evaluation of lung structure and disease primarily relies on CT and radiographic imaging. CT can provide thin-section volumetric imaging at fast acquisition speeds. MRI may offer additional soft-tissue characterization with adaptable image weighting (eg, T1, T2). In the lung, however, structural proton MRI suffers from low proton density and susceptibility gradient artifacts, thereby hampering the attainable image quality. Moreover, when compared with CT, MRI provides lower spatial resolution and requires long examination times. Despite substantial technical advances, the clinical role of structural MRI in lung imaging remains limited.

Recent developments in ultrashort echo time (UTE) gradient-echo imaging at 1.5 T and 3 T have generated promising T1-weighted images (1,2). UTE imaging has been used to assess several lung diseases, including small nodules (3,4). Moreover, MRI has been used to garner useful tissue characterization, especially in lung cancer (5–7). T2-weighted MRI, which is commonly used in abdominal imaging to detect edema, masses, and inflammation, has had limited application in the lung, however. Few studies have explored T2-weighted pulmonary imaging using turbo spin-echo (TSE) imaging and half-Fourier acquired single-shot TSE (8–12).

We recently described a prototype low-field-strength MRI system with contemporary hardware and software capabilities and demonstrated the feasibility of lung MRI using this system (13). While many low-field-strength MRI systems use permanent magnet or electromagnet designs and open-bore configurations, this system uses a closed-bore superconducting magnet design operating at 0.55 T. This magnet design provides superior field homogeneity compared with contemporary clinical MRI systems (1.5 T and 3 T) and most implementations of low-field-strength MRI systems. At 0.55 T, parenchymal T2* is approximately 10 msec, compared with T2* of less than 2 msec at 1.5 T (13). This improved field homogeneity and prolonged T2* can be exploited to reduce susceptibility artifacts in the lung parenchyma on MR images. In addition, T1 relaxation is shorter at lower field strength (lung parenchyma T1, 970 msec at 0.55 T), which is valuable for efficient sequence design, and T2 tends to be somewhat longer (lung parenchyma T2, 60 msec at 0.55 T) (13). Other contemporary elements of this system include the receiver chain, phased-array coil technology, and a fast high-fidelity gradient subsystem.

For the study reported herein, we applied a TSE acquisition for structural T2-weighted imaging of the

Abbreviations

TSE = turbo spin-echo, UTE = ultrashort echo time

Summary

A 0.55-T MRI system with contemporary hardware and software capabilities generated excellent image quality for common lung abnormalities, with image interpretations that agreed well with those of CT.

Key Points

- New low-field-strength MRI systems equipped with contemporary technology can yield high-quality images of the lung parenchyma because of the improved field homogeneity and prolonged T2*.
- This small study compared T2-weighted MRI with CT over a range of common lung abnormalities, including bronchiectasis, consolidative opacities, cystic disease, cavitary lesions, and nodules as small as 5 mm.
- Interpretation of MR images agreed strongly with interpretation of CT images for large imaging findings (R^2 = 0.99 for 5–23-mm nodules) and agreed moderately with interpretation of CT images for smaller diffuse imaging findings.

Keywords

MRI, Pulmonary, Technology Assessment

lung, exploiting the favorable imaging properties of our 0.55-T MRI system. We report findings in a small participant sample to demonstrate the structural imaging capabilities of this new MRI platform compared with CT imaging in patients with common types of lung disease.

Materials and Methods

Study Participants

Patients with lung disease were recruited to undergo research MRI between November 2018 and December 2019. This prospective Health Insurance Portability and Accountability Act–compliant imaging study was approved by our local institutional review board (clinicaltrials.gov NCT03331380). Each patient provided written informed consent. A total of 24 patients (mean age, 59 years ± 16 [standard deviation]; 18 women) underwent imaging in this MRI structural lung imaging pilot study. There were 23 patients with common pulmonary disease, including bronchiectasis, consolidations, and known lung nodules, identified by the study team using previously acquired CT images and who subsequently underwent MRI. One additional patient with lymphangioleiomyomatosis, a rare cystic lung disease mostly affecting women, was included in this sample to demonstrate the imaging capabilities of this low-field-strength MRI system in cystic disease. The imaging data from this patient were neither read nor scored but were included for illustrative purposes. All participants also underwent clinically indicated CT imaging evaluation within 119 days (median, 4 days; interquartile range, 0–34 days).

0.55-T MRI Examination

A clinical 1.5-T MRI system modified to operate at 0.55 T was used for imaging (prototype Magnetom Aera; Siemens Healthineers). Lung imaging was performed with an 18-channel spine phased-array coil and a six-channel body phased-array coil for 0.55 T. We used a free-breathing, respiratory-triggered Cartesian TSE sequence for T2-weighted imaging (typical parameters: repetition time, respiration rate; echo time, 47 msec; echo spacing, 7.86 msec; turbo factor, seven; echo trains per section, 16; field of view, 270 mm × 360 mm; matrix, 214 × 320; section thickness, 6 mm with 1.2-mm section gap; spatial resolution, 1.2 mm × 1.2 mm × 6 mm; 32 axial sections; four signal averages; receiver bandwidth, 260 Hz/pixel; and generalized autocalibrating partially parallel acquisition [GRAPPA] acceleration rate, two). Respiratory triggering was performed by using a navigator placed over the liver dome, which triggered the acquisition during expiration. Five respiratory cycles were used to learn the respiratory pattern; the acquisition window was 35% of the respiratory period, with an acceptance window of ± 2 mm diaphragm position. Each group of images was acquired over 64 respiratory cycles for four signal averages, and sections were concatenated into two or three groups, adapted to the variable respiration rate.

CT Imaging

CT images were acquired using conventional CT systems (Aquilion One Genesis edition; Canon Medical Systems; Somatom Force, Siemens Healthineers). Volumetric CT imaging used a 512 × 512 image matrix; and approximately 400-mm field of view; 0.8 × 0.8 mm spatial resolution; 2-mm section thickness with a 1-mm interval; 2.8 CT pitch; bl64d standard clinical reconstruction kernel; and 100-kVp tube potential, with tube current modulated based on scout image attenuation. CT images were acquired at inspiration during a 5-second patient breath hold and used a median effective dose of 2.3 mSv (interquartile range, 1.8–3.2 mSv). For qualitative image comparison, CT images were reformatted to match MR image orientation and section thickness (6 mm) using a Vitrea workstation (Vital Images).

Image Interpretation and Image Quality Scores

Of 23 patients who underwent MRI interpretation, one data set (4%) was rejected owing to receiver coil hardware malfunction, and four data sets (17%) were rejected owing to respiratory artifacts. The remaining 18 data sets were assessed by the radiologists. MR images were read for common radiologic findings by three experts (M.Y.C., A.A.M., and E.C.J.) with 8, 9, and 30 years of experience, respectively, reading chest CT images and 11, 15, and 25 years of experience, respectively, reading MR images. Readers were blinded to the clinical data, CT images, and CT clinical reports. Each reader independently evaluated the MRI data and provided binary assessment of the following features: scattered nodules, tree-in-bud opacities, ground-glass opacities, cavitation, bronchiectasis or bronchial wall thickening, consolidation, atelectasis or scarring, mucus plug, and pleural effusion. If there was a discrepancy between readers, the majority interpretation (two of three readers) was selected. MRI findings were compared

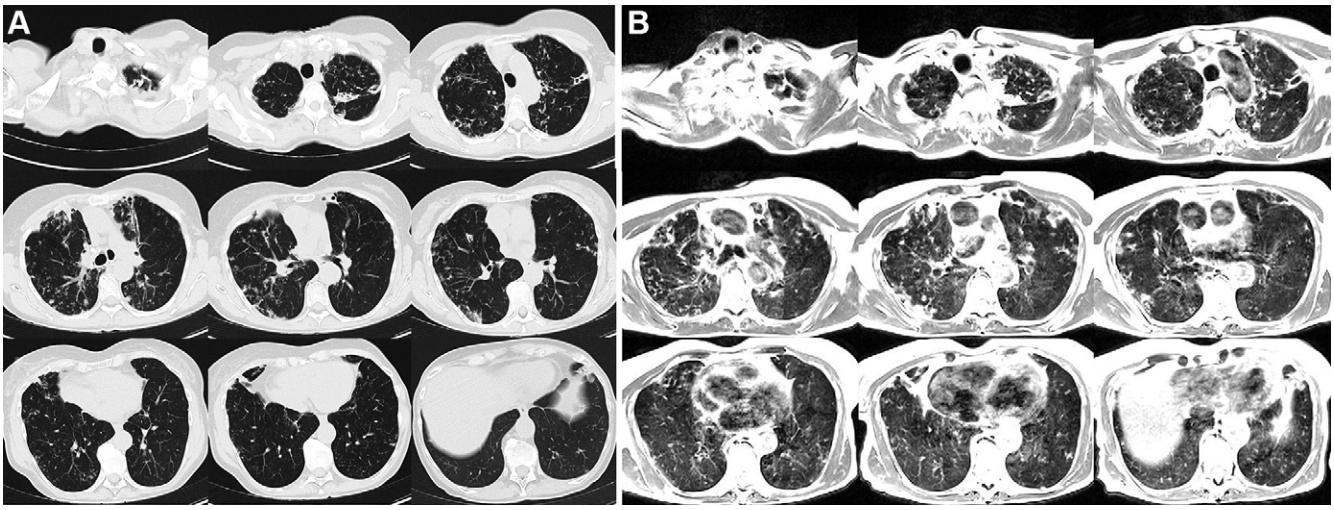

Figure 1: Axial multisection imaging yielded full lung coverage using **(A)** CT (reformatted to 0.8 × 0.8 × 6 mm) and **(B)** T2-weighted MRI (1.1 × 1.1 × 6 mm) in a 69-year-old woman with bronchiectasis, cavitary lesions, and scattered pulmonary nodules.

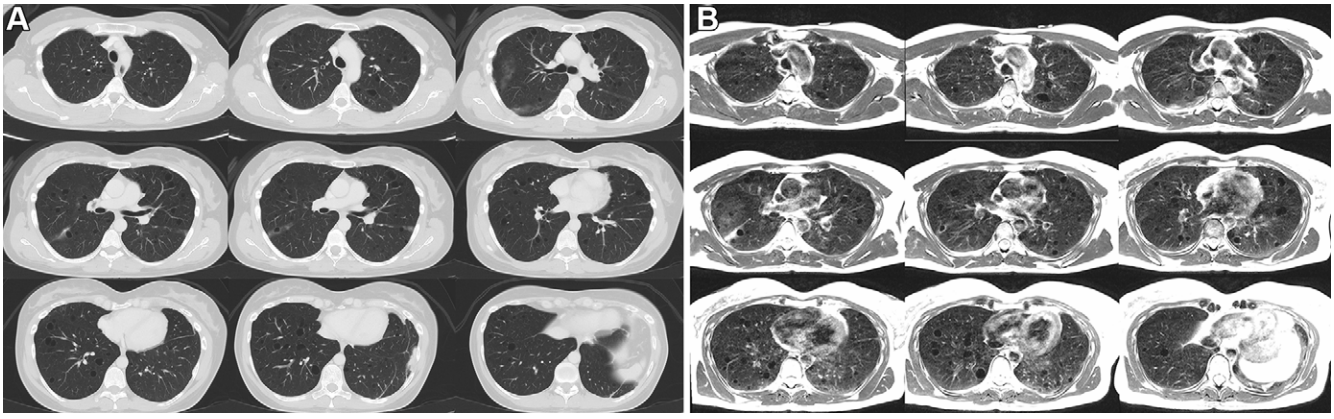

Figure 2: Axial multisection imaging yielded full lung coverage using **(A)** CT (reformatted to 0.8 × 0.8 × 6 mm) and **(B)** T2-weighted MRI (1.1 × 1.1 × 6 mm) in a 41-year-old woman with lymphangioleiomyomatosis resulting in innumerable thin-walled pulmonary cysts.

with the contemporaneous clinical CT reports. In patients with solid lung nodules, the nodule sizes were independently measured on MR and CT images for comparison.

The three readers, who were accustomed to chest CT, also scored MR image quality from 1 to 5 on a Likert-type scale (1, nondiagnostic; 2, low quality; 3, moderate quality; 4, good quality; 5, excellent quality). Both MRI artifacts and diagnostic confidence were considered in image quality scores.

Statistical Analysis

Radiologic findings from CT and MRI were compared by using the Cohen κ statistic, with κ of 0–0.2 indicating slight agreement; κ of 0.21–0.4, fair agreement; κ of 0.41–0.6, moderate agreement; κ of 0.61–0.8, substantial agreement; and κ of 0.81–1.0, almost perfect agreement. The 95% CIs of κ were calculated as ± 1.96 standard error of κ. In addition, using the CT clinical reports as the reference standard, the number of false-positive and false-negative MRI readings were also calculated. Nodule sizes measured using CT and MRI were compared using the coefficient of determination (R^2), with significant correlation defined as $P <$ .05, as well as Bland-Altman analysis. Statistical analyses were performed using Matlab (version R2020a; Mathworks).

Results

T2-weighted MRI

T2-weighted TSE MRI generated signal in the lung parenchyma and provided details of bronchial structure and vascular structure. The acquisition time for T2-weighted TSE was dependent on respiration rate and averaged 10.5 minutes ± 2.8 for 32 sections (n = 24 participants).

Figures 1 and 2 provide example T2-weighted MR images compared with matching CT sections covering the entire lung volume in two patients. In the first patient, both CT and MR images show bronchiectasis, cavitary lesions, and scattered nodules. Depiction of these lung findings was similar between the two imaging modalities. The second patient was diagnosed with lymphangioleiomyomatosis; a heavy burden of cystic lung disease was visible using both CT and MRI. Parenchymal signal is high in patients with lymphangioleiomyomatosis, which is attributed to the proliferation of smooth muscle-like cells in the lung during disease progression.

Figure 3 shows example MR images of lung nodules in three patients, with comparison with CT images reformatted to the same section thickness and image orientation. The mean nodule

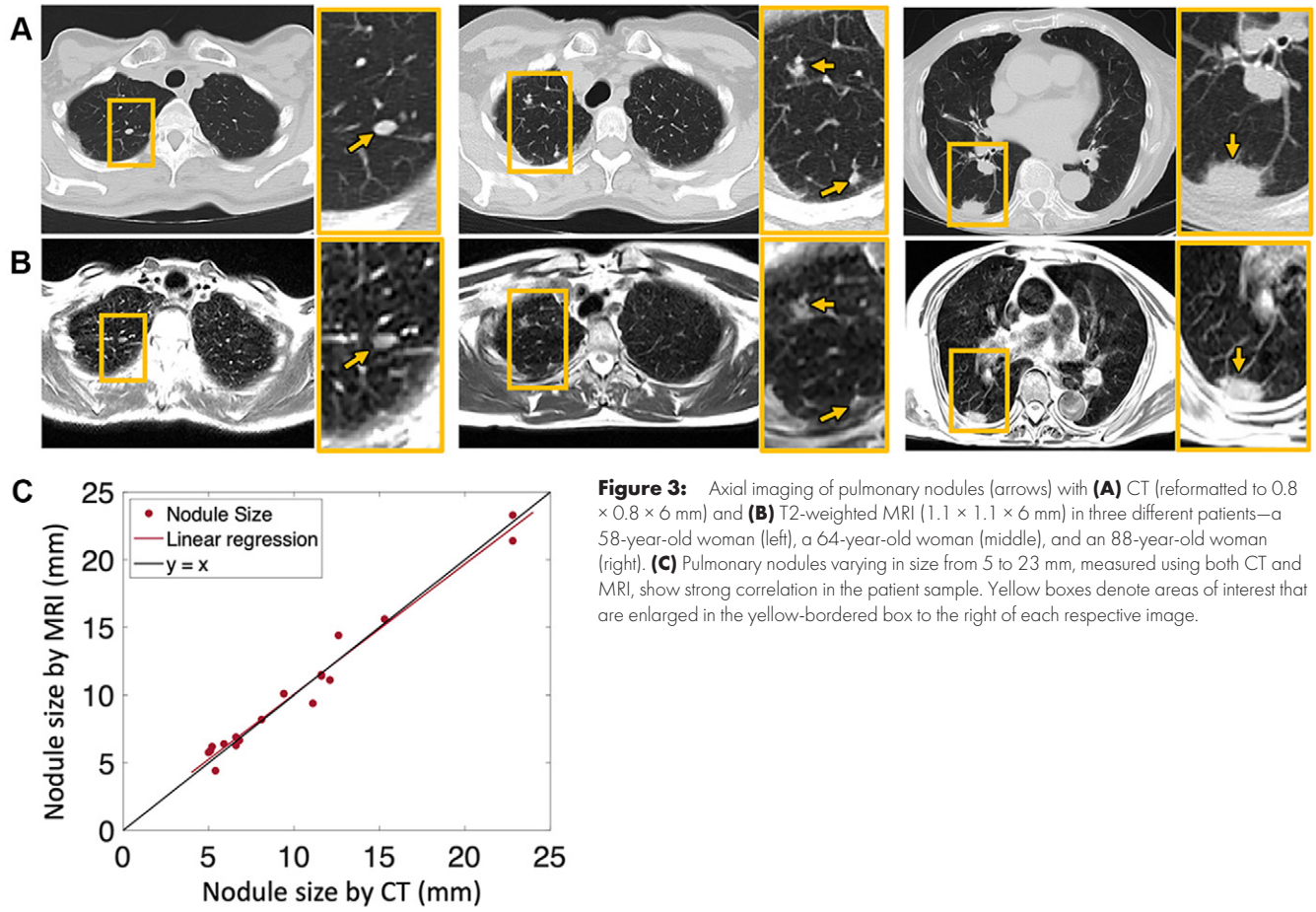

Figure 3: Axial imaging of pulmonary nodules (arrows) with **(A)** CT (reformatted to 0.8 × 0.8 × 6 mm) and **(B)** T2-weighted MRI (1.1 × 1.1 × 6 mm) in three different patients—a 58-year-old woman (left), a 64-year-old woman (middle), and an 88-year-old woman (right). **(C)** Pulmonary nodules varying in size from 5 to 23 mm, measured using both CT and MRI, show strong correlation in the patient sample. Yellow boxes denote areas of interest that are enlarged in the yellow-bordered box to the right of each respective image.

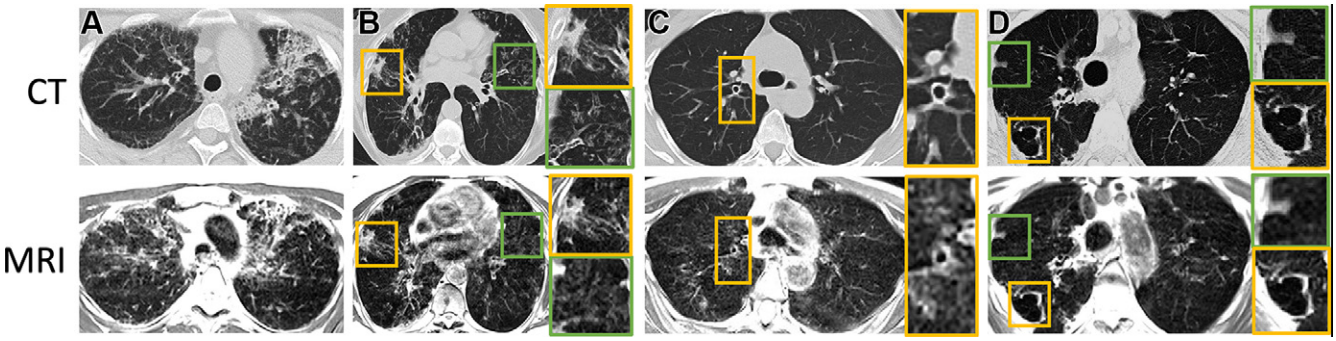

Figure 4: Axial CT (reformatted to 0.8 × 0.8 × 6 mm) and T2-weighted MR (reformatted to 1.1 × 1.1 × 6 mm) images show **(A)** honeycombing, interstitial thickening, and fibrotic changes in a 35-year-old woman; **(B)** consolidative opacities in a 70-year-old woman; **(C)** bronchial wall thickening with bronchiectasis in a 58-year-old woman; and **(D)** a cavitary lesion in a 70-year-old woman. **(B–D)** Green and yellow boxes on CT and MR images denote the area of interest around the particular finding described, with the corresponding box bordered in that color to the right of the respective image showing an enlarged view of the area.

size in this study was 10 mm ± 5 (range, 5–23 mm; 19 nodules measured in seven patients), based on both CT and MR images. We observed excellent correlation (Fig 3C) (R^2 = 0.99, $P <$ .001) between the measurements and small Bland-Altman bias (mean, 0.05 mm ± 1.75). This correlation is promising because it indicates that clinically important lung nodules larger than 6 mm could be detected and monitored using T2-weighted MRI at 0.55 T (14).

Isolated examples of bronchial wall thickening, consolidative opacities, honeycombing, interstitial thickening, fibrosis, and cavitary lesions in four different patients are provided in Figure 4. These features were reported when using clinically indicated CT, but they also were visible when using MRI. Tissue consolidations yielded high signal intensity and were well depicted with MRI.

Image Interpretation and Image Quality Scores

From 18 MRI data sets scored by three readers (total scores, 54) on a five-point scale, with 1 being nondiagnostic and 5 being excellent quality, the majority of image quality scores were deemed *good* (score of 5, n = 9; score of 4, n = 28; score of 3, n = 13; score of 2, n = 4; score of 1, n = 0). This indi-

Comparison of Clinical Findings by 0.55-T MRI and CT in 18 Patients

Parameter	No. at CT	No. at MRI	Mean κ Value	100% Consensus (MRI)*	100% Consensus (MRI and CT)†	MRI FN	MRI FP
Scattered solid nodules	14	15	0.82 (0.49, 1.16)	10 (56)	10 (56)	0	1
Tree in bud nodularity	7	3	0.48 (0.03, 0.93)	9 (50)	9 (50)	4	0
Ground-glass opacity	6	10	0.57 (0.20, 0.94)	5 (28)	5 (28)	0	4
Cavitation	3	3	1.00 (1.00, 1.00)	15 (83)	15 (83)	0	0
Bronchiectasis or bronchial wall thickening	14	16	0.61 (0.10, 1.12)	12 (67)	12 (67)	0	2
Consolidation	5	5	1.00 (1.00, 1.00)	12 (67)	12 (67)	0	0
Atelectasis or scarring	13	14	0.56 (0.10, 1.01)	11 (61)	11 (61)	1	2
Mucus plug	5	3	0.68 (0.27, 1.10)	9 (50)	9 (50)	2	0
Pleural effusion	1	2	0.64 (−0.05, 1.33)	15 (83)	15 (83)	0	1

Note.—Cohen κ statistic definitions are as follows: 0–0.2, slight agreement; 0.21–0.4, fair agreement; 0.41–0.6, moderate agreement; 0.61–0.8, substantial agreement; and 0.81–1.0, almost perfect agreement. For Cohen statistics, data in parentheses are 95% CIs. For consensus values, data are numbers of findings, with percentages (out of 18 total patients) in parentheses. FN = false negative, FP = false positive.

* Indicates there was 100% consensus between three readers for MRI findings.

† Indicates there was 100% consensus between the CT findings and all three readers for MRI findings.

cates that the majority of data sets were free from disruptive imaging artifacts and interpretation was possible with strong diagnostic confidence.

The Table provides a comparison of radiologic findings and κ score, comparing the MRI findings of the three readers to CT clinical reports. The numbers of false-positive findings, false-negative findings, and patients with consensus between MRI readers and CT reports are also provided. In general, consolidations, cavitation, mucus plug, scattered nodules, bronchiectasis or bronchial wall thickening, and pleural effusion demonstrated substantial to almost perfect agreement between MRI and CT (κ range, 0.61–1). Ground-glass opacities, tree-in-bud pattern nodularity, and scarring were less concordant between MRI and CT (moderate agreement by κ: range, 0.48–0.57). False-positive and false-negative findings were also most common (four of 18 cases) for tree-in-bud nodules and ground-glass opacities. This discrepancy might be attributable to the difference in respiratory position between MRI and CT, or it may demonstrate the suboptimal capability of MRI to detect subtle processes causing tree-in-bud and ground-glass opacities. Two false-positive readings of bronchiectasis and of scarring or atelectasis were also observed using MRI. Consensus between all three MRI readers and CT clinical reports was also highest for cavitation, bronchiectasis, effusion, and consolidation, indicating strong diagnostic confidence for these larger imaging findings. Evaluations from the three independent readers are provided as Tables E1–E3 (supplement).

Discussion

We provide a small feasibility study to assess the capabilities of 0.55-T MRI with contemporary hardware and software for T2-weighted imaging of the lung. Images from patients undergoing clinical lung CT for a variety of diseases were compared with images generated with 0.55-T MRI. Many abnormalities, including cysts, bronchial wall thickening, consolidation, and small nodules, were identified at MRI. This participant sample was used to illustrate structural lung imaging using 0.55-T MRI with an average acquisition time of 11 minutes.

One primary advantage of MRI over CT is its capability to generate soft-tissue contrast with variable contrast weighting, including T1 and T2. T1-weighted imaging and other MRI contrasts were not reported here. Flexible MRI contrast may allow characterization of tissue composition, similar to the excellent specificity provided by MRI elsewhere in the body and in previous studies of pulmonary nodules at 1.5 T and 3 T (5,7,15–18). As with any new field strength, additional sequence optimization is required to harness the full capabilities of tissue characterization at 0.55 T. In addition, MRI is advantageous over CT because it is free from ionizing radiation, which makes it especially attractive for repeated lung imaging and pediatric imaging. In this study, a median effective dose of 3.2 mSv was reported from CT examinations.

We chose to use a 0.55-T MRI system to reduce image artifacts caused by susceptibility gradients at air-tissue interfaces. Most commercial low-field-strength (<1.5 T) MRI systems use permanent magnet design (19); however, our 0.55-T system uses a superconductive magnet design, operating at a lower field strength. As a result, absolute field homogeneity is improved compared with higher-field systems and nonsuperconducting low-field-strength systems, and susceptibility artifacts are less problematic. In a previous study of this 0.55-T MRI system, T2* in the lung at 0.55 T was measured to be 10 msec, and T2 was measured to be 60 msec (13).

Although many proton imaging applications in the lung rely on UTE imaging (20,21), we used a longer echo time of 47 msec with a TSE sequence to generate T2 weighting. This echo time is similar to that used for T2 weighting in the abdomen. Despite the long echo time, we were able to preserve parenchymal signal and

mitigate signal loss. We selected TSE over half-Fourier acquired-single-shot TSE for higher signal-to-noise ratio. Respiratory triggering was performed using signal from a navigator placed over the liver dome, and in four patients severe respiratory motion artifacts corrupted the images. Future work will focus on eliminating motion artifacts that can disrupt image quality. Respiratory-triggered T2-weighted MRI was also performed in expiration, and expiratory imaging is known to be disadvantageous for lung parenchymal imaging with both MRI and CT (22).

At 1.5 T and 3 T, most research has focused on hyperpolarized gas MRI, which provides substantial value for imaging regional lung function (23), and on UTE imaging for routine T1-weighted imaging of the lung structure. A few studies have achieved moderate success with T2-weighted structural imaging on commercially available 1.5-T and 3-T MRI systems. Lower parenchymal signal has been observed in these previous studies, which limits the detection of certain diseases (9). Zeng et al (8) used high-quality motion-corrected T2-weighted TSE MRI at 1.5 T to detect lung abnormalities in 63 patients with tuberculosis. In general, the delineation of features using 0.55-T MRI shows promising image quality relative to previous reports of T2-weighted lung MRI.

There were several limitations to this pilot study. Respiratory triggering using a navigator placed over the liver dome was only moderately successful and resulted in respiratory artifacts on images. In the future, more sophisticated methods to compensate for motion will be explored (24). No compensation for cardiac motion was applied in this study, and artifacts are visible on some lung images. Our prototype 0.55-T MRI system used custom receiver coils with limited coverage (six-channel anterior body array, 18-channel spine coil). These coils were retuned from 1.5 T and therefore did not perform optimally at 0.55 T. Moreover, the limited coil coverage and coil penetration were challenging for imaging patients with large body habitus. The small number of channels limited the parallel imaging capabilities, and here we only used a GRAPPA rate of two. MR image acquisition required a mean of 11 minutes and generated anisotropic resolution, which does not allow three-dimensional image reformatting. Diffuse radiologic findings, such as ground-glass opacities and tree-in-bud nodules, were challenging to detect in the current study. In this small initial study, we compared CT images acquired at inspiration with MR images acquired at expiration, rather than at the same respiratory phase, which likely contributed to the discrepancy between the two modalities when evaluating diffuse disease. Diffuse disease may also be less demonstratable using 6-mm section thickness for either CT or MRI, and future work will optimize MRI sequences for higher section resolution. Improved motion robustness and resolution may also be beneficial to detect these features in the future. Our study included a small number of patients; therefore, additional validation is required to demonstrate the clinical value of 0.55-T MRI for routine imaging.

In conclusion, we have presented, to our knowledge, the first pilot study of T2-weighted lung MRI using a 0.55-T MRI system with contemporary hardware and software capabilities. Our findings in this small sample of patients indicate excellent image quality that shows promise for clinical diagnosis and evaluation of common lung disease.

Acknowledgments: We acknowledge the assistance of Siemens Healthineers in the modification of the MRI system for operation at 0.55 T under an existing cooperative research agreement (CRADA) between NHLBI and Siemens Healthineers. We also acknowledge Waqas Majeed and Pedro Itriago Leon from Siemens Healthineers for their assistance in protocol optimization at 0.55 T. We acknowledge the contributions of Delaney McGuirt, Christine Mancini, Kendall O'Brien, Margaret (Peg) Lowery, and Jennifer Henry. We thank Dr Robert Lederman for acting as medically accountable investigator on the clinical protocol.

Author contributions: Guarantor of integrity of entire study, A.E.C.W.; study concepts/study design or data acquisition or data analysis/interpretation, all authors; manuscript drafting or manuscript revision for important intellectual content, all authors; approval of final version of submitted manuscript, all authors; agrees to ensure any questions related to the work are appropriately resolved, all authors; literature research, A.E.C.W.; clinical studies, all authors; statistical analysis, A.E.C.W.; and manuscript editing, A.E.C.W., A.A.M., J.M., K.P.F., M.Y.C.

Disclosures of Conflicts of Interest: **A.E.C.** disclosed no relevant relationships. **A.A.M.** disclosed no relevant relationships. **E.C.J.** disclosed no relevant relationships. **J.M.** disclosed no relevant relationships. **K.P.F.** disclosed no relevant relationships. **K.N.O.** Activities related to the present article: disclosed no relevant relationships. Activities not related to the present article: received a grant from Beyond Air. Other relationships: disclosed no relevant relationships. **M.Y.C.** disclosed no relevant relationships.

References

1. Zhu X, Chan M, Lustig M, Johnson KM, Larson PEZ. Iterative motion-compensation reconstruction ultra-short TE (iMoCo UTE) for high-resolution free-breathing pulmonary MRI. Magn Reson Med 2020;83(4):1208–1221.
2. Dournes G, Yazbek J, Benhassen W, et al. 3D ultrashort echo time MRI of the lung using stack-of-spirals and spherical k-Space coverages: Evaluation in healthy volunteers and parenchymal diseases. J Magn Reson Imaging 2018;48(6):1489–1497.
3. Wielpütz MO, Lee HY, Koyama H, et al. Morphologic Characterization of Pulmonary Nodules With Ultrashort TE MRI at 3T. AJR Am J Roentgenol 2018;210(6):1216–1225.
4. Burris NS, Johnson KM, Larson PE, et al. Detection of Small Pulmonary Nodules with Ultrashort Echo Time Sequences in Oncology Patients by Using a PET/MR System. Radiology 2016;278(1):239–246.
5. Kurihara Y, Matsuoka S, Yamashiro T, et al. MRI of pulmonary nodules. AJR Am J Roentgenol 2014;202(3):W210–W216.
6. Meier-Schroers M, Homsi R, Schild HH, Thomas D. Lung cancer screening with MRI: characterization of nodules with different non-enhanced MRI sequences. Acta Radiol 2019;60(2):168–176.
7. Koyama H, Ohno Y, Seki S, et al. Magnetic resonance imaging for lung cancer. J Thorac Imaging 2013;28(3):138–150.
8. Zeng J, Liu Z, Shen G, et al. MRI evaluation of pulmonary lesions and lung tissue changes induced by tuberculosis. Int J Infect Dis 2019;82:138–146.
9. Eibel R, Herzog P, Dietrich O, et al. Pulmonary abnormalities in immunocompromised patients: comparative detection with parallel acquisition MR imaging and thin-section helical CT. Radiology 2006;241(3):880–891.
10. Schroeder T, Ruehm SG, Debatin JF, Ladd ME, Barkhausen J, Goehde SC. Detection of pulmonary nodules using a 2D HASTE MR sequence: comparison with MDCT. AJR Am J Roentgenol 2005;185(4):979–984.
11. Leutner CC, Gieseke J, Lutterbey G, et al. MR imaging of pneumonia in immunocompromised patients: comparison with helical CT. AJR Am J Roentgenol 2000;175(2):391–397.
12. Bruegel M, Gaa J, Woertler K, et al. MRI of the lung: value of different turbo spin-echo, single-shot turbo spin-echo, and 3D gradient-echo pulse sequences for the detection of pulmonary metastases. J Magn Reson Imaging 2007;25(1):73–81.
13. Campbell-Washburn AE, Ramasawmy R, Restivo MC, et al. Opportunities in Interventional and Diagnostic Imaging by Using High-Performance Low-Field-Strength MRI. Radiology 2019;293(2):384–393.
14. MacMahon H, Naidich DP, Goo JM, et al. Guidelines for Management of Incidental Pulmonary Nodules Detected on CT Images: From the Fleischner Society 2017. Radiology 2017;284(1):228–243.
15. Liu H, Liu Y, Yu T, Ye N. Usefulness of diffusion-weighted MR imaging in the evaluation of pulmonary lesions. Eur Radiol 2010;20(4):807–815.
16. Mori T, Nomori H, Ikeda K, et al. Diffusion-weighted magnetic resonance imaging for diagnosing malignant pulmonary nodules/masses: comparison with positron emission tomography. J Thorac Oncol 2008;3(4):358–364.
17. Schaefer JF, Vollmar J, Schick F, et al. Solitary pulmonary nodules: dynamic contrast-enhanced MR imaging--perfusion differences in malignant and benign lesions. Radiology 2004;232(2):544–553.

18. Henzler T, Schmid-Bindert G, Schoenberg SO, Fink C. Diffusion and perfusion MRI of the lung and mediastinum. Eur J Radiol 2010;76(3):329–336.
19. Marques JP, Simonis FFJ, Webb AG. Low-field MRI: An MR physics perspective. J Magn Reson Imaging 2019;49(6):1528–1542.
20. Johnson KM, Fain SB, Schiebler ML, Nagle S. Optimized 3D ultrashort echo time pulmonary MRI. Magn Reson Med 2013;70(5):1241–1250.
21. Zha W, Kruger SJ, Johnson KM, et al. Pulmonary ventilation imaging in asthma and cystic fibrosis using oxygen-enhanced 3D radial ultrashort echo time MRI. J Magn Reson Imaging 2018;47(5):1287–1297.
22. Bankier AA, O'Donnell CR, Boiselle PM. Quality initiatives. Respiratory instructions for CT examinations of the lungs: a hands-on guide. RadioGraphics 2008;28(4):919–931.
23. Mugler JP III, Altes TA. Hyperpolarized 129Xe MRI of the human lung. J Magn Reson Imaging 2013;37(2):313–331.
24. Jiang W, Ong F, Johnson KM, et al. Motion robust high resolution 3D free-breathing pulmonary MRI using dynamic 3D image self-navigator. Magn Reson Med 2018;79(6):2954–2967.